ISSN 0145-8752, Moscow University Geology Bulletin, 2024, Vol. 79, No. 1, pp. 70–79. © Allerton Press, Inc., 2024.
Russian Text © The Author(s), 2023, published in Vestnik Moskovskogo Universiteta, Seriya 4: Geologiya, 2023, No. 6, pp. 67–76.

Radioactivity of Surface Marine Sediments of Chaun Bay: Analysis of Natural and Anthropogenic Factors

A. S. Ulyantsev[a, *] (ORCID: 0000-0003-2230-1069), S. I. Ivannikov[b, **] (ORCID: 0000-0002-5889-3409), S. Yu. Bratskaya[b, *] (ORCID: 0000-0003-4954-0422), and A. N. Charkin[c, ****] (ORCID: 0000-0001-9273-9950)**

[a] *Shirshov Institute of Oceanology, Russian Academy of Sciences, Moscow, 117997 Russia*
[b] *Institute of Chemistry, Far Eastern Branch, Russian Academy of Sciences, Vladivostok, 690022 Russia*
[c] *Il'ichev Pacific Oceanological Institute, Far Eastern Branch, Russian Academy of Sciences, Vladivostok, 690041 Russia*
**e-mail: uleg85@gmail.com*
***e-mail: yajkfqn@mail.ru*
****e-mail: s.bratskaya@gmail.com*
*****e-mail: charkin@poi.dvo.ru*

Received September 20, 2023; revised October 2, 2023; accepted January 22, 2024

Abstract—The paper presents data on the spatial distribution of the active concentration of natural (^{232}Th, ^{226}Ra, and ^{40}K) and anthropogenic (^{137}Cs) radionuclides in the surface layer of bottom sediments in Chaun Bay of the East Siberian Sea. The measured active concentration of ^{232}Th and ^{226}Ra was typical of bottom sediments of the Arctic coastal shelf zone and corresponded to the global level. The level of ^{137}Cs activity in bottom sediments showed the absence of local sources of anthropogenic pollution in Chaun Bay, while the mean ^{40}K activity concentration was 1.8 times higher than the global. The results of statistical analysis of the data obtained showed that the dynamics of river runoff, thermal abrasion, and currents, as well as aeolian and ice transport of sedimentary matter, were the main factors that determined the differences in the behavior of the studied radionuclides in the surface bottom sediments of Chaun Bay.

Keywords: Arctic, marine sediments, gamma-ray spectrometry, natural radionuclides, radiocesium, factor analysis

DOI: 10.3103/S0145875224700078

INTRODUCTION

The Arctic is an area of priority national interests of Russia, the development of which directly depends on the knowledge of this complex natural system. The relevance of studying the coastal zone of Russia's Arctic seas is determined by current climate change in the Arctic, which contributes to permafrost discharge, thermal abrasion and coastal erosion, bottom degassing, and ice gouging (Vonk et al., 2012; Lobkovsky et al., 2013; Overduin et al., 2014; Gunther et al., 2015; Dudarev et al., 2016; Shakhova et al., 2017; Bröder et al., 2019). At the same time, monitoring pollution, including radioactive contamination, is of current importance in the development of the Arctic area and operation of the Northern Sea Route.

The active concentration of natural radionuclides (e.g., ^{232}Th, ^{40}K, and ^{226}Ra), as well as their ratios, are informative indicators of geological and geochemical processes in the ocean (e.g., Abril and Fraga, 1996; Ligero et al., 2001; Domanov et al., 2014, 2019; Abassi et al., 2020; Charkin et al., 2022). In marine sediments, radioisotopes of thorium, radium, and potassium are usually included in the crystal lattice of minerals and can be adsorbed directly from the water column on clay particles (Abril and Fraga, 1996; Ligero et al., 2001) or associated with organic matter (OM) (Domanov et al., 2014, 2019). Accordingly, variations in the concentration of natural radionuclides in sediments are associated with differences in their lithological composition, as well as the composition and concentration of OM. At the same time, the concentration of radiocesium (^{137}Cs) in sediments reflects anthropogenic pollution of the marine environment (Miroshnikov, 2012; Miroshnikov et al., 2017, 2020a, 2020b; Sarkisov, 2019). At present, the behavior of radiocesium and its distribution in sediments is actively studied to assess the potential hazard in the marine environment (e.g., Alshahri, 2017; Abassi et al., 2019, 2022; Nguyen et al., 2020; Mehnati et al., 2022), including the Arctic (Sarkisov, 2019; Miroshnikov et al., 2020a, 2020b; Budko et al., 2022; Yushin et al., 2023). In addition, an increased anthropogenic impact on the Arctic Ocean is associated with the commissioning of the first Russian floating nuclear power plant (Akademik Lomonosov), based in the port of Pevek in Chaun Bay of the East Siberian Sea. Thus, the main goal of this study was to determine the features of the spatial distribution of the active con-

centration of natural (^{232}Th, ^{226}Ra, and ^{40}K) and anthropogenic (^{137}Cs) radionuclides in the surface marine sediments of Chaun Bay, as well as to assess their relationship with the particle size distribution and concentration of OM.

MATERIALS AND METHODS

This study concerned bottom sediments collected at 25 stations during cruise 60 of the R/V *Akademik Oparin* in Chaun Bay (Ulyantsev et al., 2021). An Ekman-type box grab sampler (0.5 × 0.5 × 1.0 m) was used to collect material from the vessel. In shallow water, bottom sediments were collected with a Van Veen type grab sampler (25 × 15 × 15 cm) from a Chirok-320T motor-equipped rowboat. The top 10 cm layer of bottom sediments was collected for analysis. Samples for particle size analysis (10–20 g of wet sediment) were collected in polypropylene bags and stored at +4°C until laboratory analysis. To determine the concentration of organic carbon (C_{org}), 10–20 g of wet sediment was collected in polypropylene bags and stored at –18°C. For analyses, samples were lyophilized and ground using a ball mill. For gamma spectrometric analysis of radionuclide activity, approximately 1.5 kg of wet sediment was collected in stainless steel containers and dried to constant weight at +50°C for 48 h. The station layout is shown in Fig. 1.

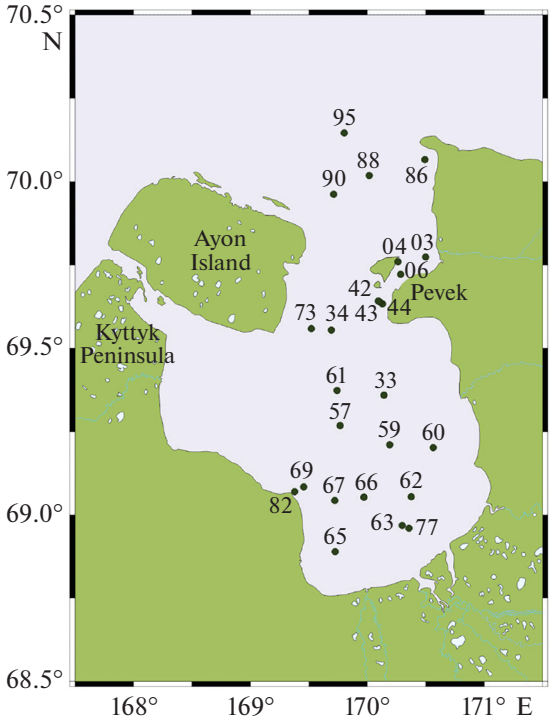

Fig. 1. Sketch map of location of bottom sediment sampling stations in Chaun Bay.

Particle size analysis of sediments was carried out in wet samples using laser diffraction after wet sieving of the sand fraction (Ulyantsev et al., 2020). A sample (2–3 g) was placed in a measuring glass; distilled water (20 mL) and 0.7% sodium hexametaphosphate solution (20 mL) were added, and the sample was left for a day. The sand fraction was separated on a sieve with a hole diameter of 0.063 mm. After that, it was sieved into fractions of 0.063–0.125, 0.125–0.25, 0.25–0.5, 0.5–1, 1–2, and >2 mm. The fractions separated in this way were dried to a constant mass and weighed with an accuracy of 0.01 g. The mass distribution of particles finer than 63 μm was determined using a SALD 2300 particle analyzer (Shimadzu, Japan) and a liquid dispersion module with constant stirring after ultrasonic exposure. Dispersant and background liquid: distilled water. The C_{org} concentration was determined in dried and crushed sediment samples by the high-temperature combustion method using a TOC-LCPN analyzer (Shimadzu, Japan). The measurement accuracy was ±3% based on the results of three parallel measurements.

Radionuclide activity was measured using a gamma spectrometric complex, including an SBS-75 measurement unit (Grin Star Tekhnolodzhiz, Russia) and a GC2018 semiconductor germanium detector (Canberra, United States). The relative efficiency of detecting the complex at the 1332 keV peak was 20%. The full width at half-maximum (FWHM) of the complex at the peak was 1332 keV = 1.8 keV. The volume of samples used for analysis was from 500 to 1000 mL. The Marinelli measurement geometry was used. Specific activity was measured with eSBS software (version 1.5.9.3). The measurement results were processed with Gamma Analyzer for Semiconductor Detectors (SCD) software (v. 1.0). To calibrate the gamma spectrometer, closed reference point sources of gamma radiation of the OSGI-3-2 type (^{60}Co, ^{137}Cs, ^{241}Am, ^{152}Eu, ^{22}Na, and ^{133}Ba) were used, located directly at the end of the detector.

For ^{226}Ra, the activity of natural radionuclides was determined by the following products: ^{214}Pb (351.9 keV) and ^{214}Bi (609.3 and 1120.3 keV); for ^{232}Th, it was determined by the lines ^{214}Pb (238.6 keV), ^{208}Tl (583.3 keV), and ^{228}Ac (911.0 and 969.0 keV); for ^{40}K, according to the 1460.7 keV line. The activity of radiocesium (^{137}Cs) was determined by the energy of its gamma radiation (661.6 keV). The measurement error depending on the intensity of the gamma lines of the determined radionuclides was within 1–7%. The specific activity of ^{226}Ra, ^{232}Th, ^{40}K, and ^{137}Cs in samples was calculated using the following formula:

$$A = \frac{N_e}{\varepsilon_f P_\gamma t_C M},$$

where N_e was the number of pulses at the total absorption peak for energy E; ε_f was the detector efficiency at energy E; P_γ was the probability of gamma radiation emission (gamma output) at energy E; t_C was sample measurement time; M was the mass of the sample.

Table 1. Coordinates of sampling stations, data on particle size distribution, and C_{org} concentration in the studied bottom sediments of Chaun Bay

Station	Latitude, N	Longitude, E	Mass content of fractions, %				C_{org}, %
			>63 μm	10–63 μm	2–10 μm	<2 μm	
03	69.772	170.503	27.58	35.50	25.51	11.41	1.20
04	69.759	170.266	2.31	27.95	47.73	22.01	2.00
06	69.720	170.288	9.76	32.36	39.11	18.77	2.60
33	69.358	170.146	2.93	35.90	42.13	19.04	2.30
34	69.554	169.695	2.18	35.26	41.21	21.35	2.10
42	69.640	170.098	9.64	32.03	39.84	18.49	1.97
43	69.637	170.112	18.44	37.31	30.02	14.23	1.70
44	69.632	170.132	8.57	40.37	34.19	16.87	1.89
57	69.267	169.772	5.73	28.73	42.94	22.60	2.11
59	69.209	170.195	6.67	43.22	33.28	16.83	1.87
60	69.201	170.569	7.99	64.13	19.87	8.01	1.69
61	69.372	169.744	0.75	29.09	49.45	20.71	2.39
62	69.053	170.380	9.07	60.21	21.59	9.13	1.93
63	68.967	170.302	75.80	14.36	6.46	3.38	0.51
65	68.888	169.728	74.93	23.64	1.02	0.41	0.33
66	69.052	169.974	8.79	42.86	31.55	16.80	1.61
67	69.043	169.726	32.33	40.26	17.55	9.86	1.21
69	69.082	169.460	64.10	23.42	8.54	3.94	0.59
73	69.558	169.523	62.47	19.98	11.48	6.07	0.42
77	68.958	170.358	57.27	29.28	8.92	4.53	0.68
82	69.065	169.359	96.33	3.67	0.00	0.00	1.01
86	70.064	170.497	3.08	31.26	43.34	22.32	1.75
88	70.017	170.020	23.77	44.88	20.19	11.16	1.09
90	69.961	169.714	20.87	43.52	23.06	12.55	1.33
95	70.145	169.807	9.85	47.09	27.45	15.61	1.13

If there was more than one peak for a radionuclide in the energy range, the specific activity was averaged by calculating the weighted average value. To reduce the statistical error, the sample was irradiated for 54000 s. Background spectra for an empty sealed Marinelli beaker were recorded under the same conditions and were used to correct the area of the gamma radiation peaks of the measured radionuclides. The background was subtracted for each energy transition.

BRIEF DESCRIPTION OF THE STUDY AREA

Chaun Bay is located in the southeastern part of the East Siberian Sea; it is a polygonal bay with northwestern spatial orientation and many small rivers flowing into it (Stremyakov, 1963). It is distinguished by its relative isolation from open water; it extends into the mainland for more than 100 km and reaches a maximum width of 95 km. The polygonal tundra landscape is developed in the western (Ayon Island and Kyttyk Peninsula) and southern parts, in which numerous thermokarst lakes, alases, and small rivers are concentrated. The western shore is low-lying, while the eastern shore is more elevated (*Ekosistemy*..., 1994).

PARTICLE SIZE DISTRIBUTION IN SEDIMENTS AND C_{org}

Data on the particle size distribution and C_{org} in the studied bottom sediments are shown in Table 1. The mass concentration of sand (>63 μm), coarse (10–63 μm) and fine (2–10 μm) silt, as well as clay (<2 μm), in the studied bottom sediments ranged from 0.75 to 96.33 (mean, 25.65%), 3.67 to 64.13 (mean 34.65%), 0.00 to 49.45 (mean 26.66%), and 0.00 to 22.60 (mean 13.04%), respectively; C_{org} concentration varied from 0.33 to 2.60% (average, 1.50%). The maximum C_{org} concentrations were observed in the central area of Chaun Bay, in which fine-grained sediments were common. Lower C_{org} concentrations corresponded to sandy and silty-sandy sediments. In general, the nature of the distribution of C_{org} in sediments

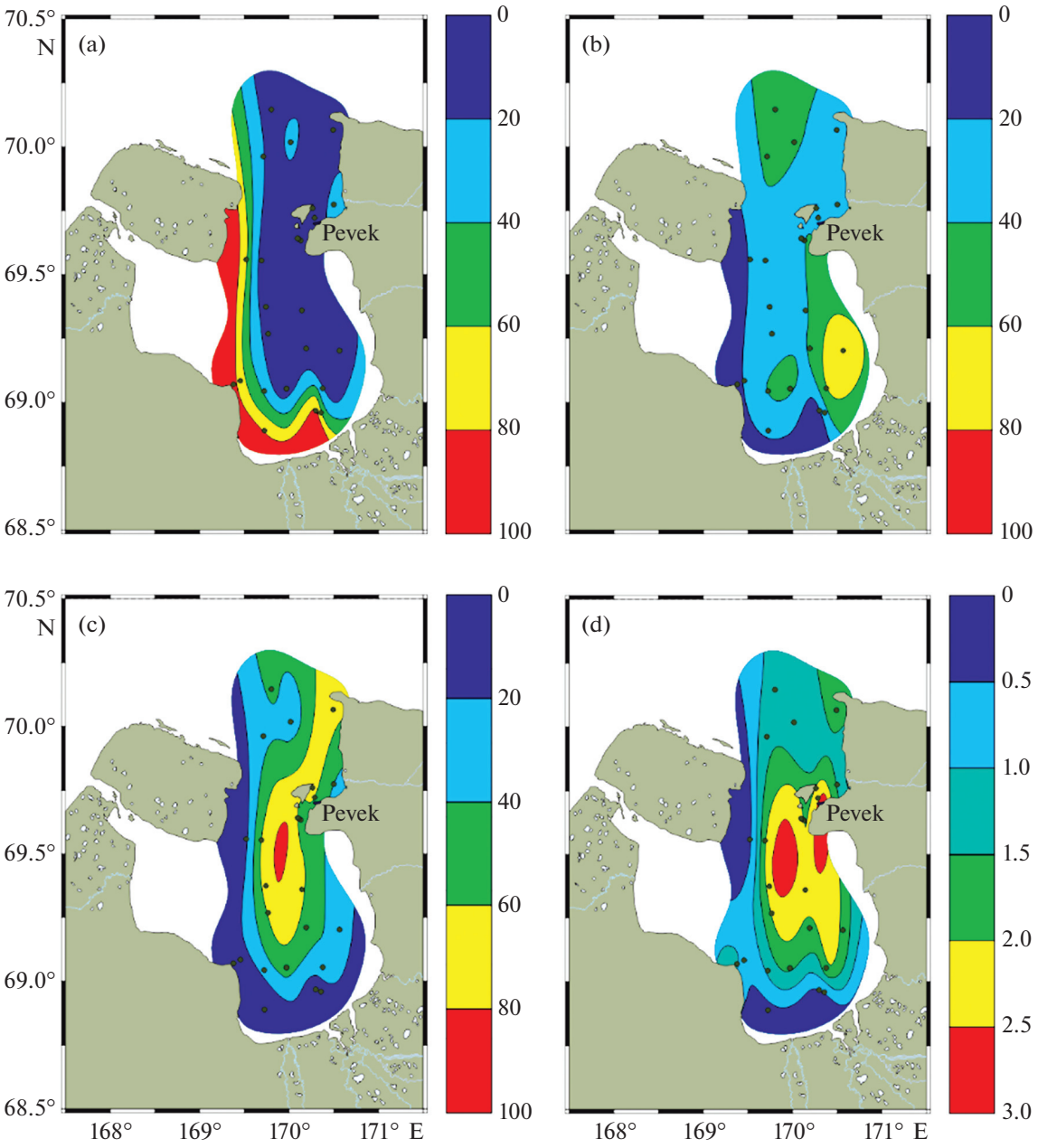

Fig. 2. Surface distributions of mass content of size fractions >63 μm (a), 10–63 μm (b), sum of 2–10 + <2 μm (c), and C_{org} concentration (d) in studied bottom sediments.

agreed with their particle size distribution (Fig. 2), which was statistically confirmed.

The western and southern parts of the bay contained the most coarse-grained sediments. In the western part of the bay, the particle size distribution of sediments was affected by the dynamics of thermal abrasion of polygonal-tundra permafrost deposits that were widely developed there. The latitudinal distribution of sediments was associated with the impact of the current coming from the north (*Ekosistemy*..., 1994). The southern part of Chaun Bay was more exposed to the influence of river runoff, which also carried a significant amount of thermal abrasion products. As in the western part of the bay, sediments of sandy and silty-sandy sizes were common there. In the eastern part of Chaun Bay, silt-sized sediments were concentrated. As in the case of coarse-grained sediments, the distribution of silts was associated with the dynamics of river runoff, thermal abrasion, and currents, while the observed spatial fluctuations were probably associated with the impact of seasonal ice discharge and aeolian transport of sedimentary matter.

In the central part of the bay and at the outlet to the East Siberian Sea, sediments of silty-clayey and clayey

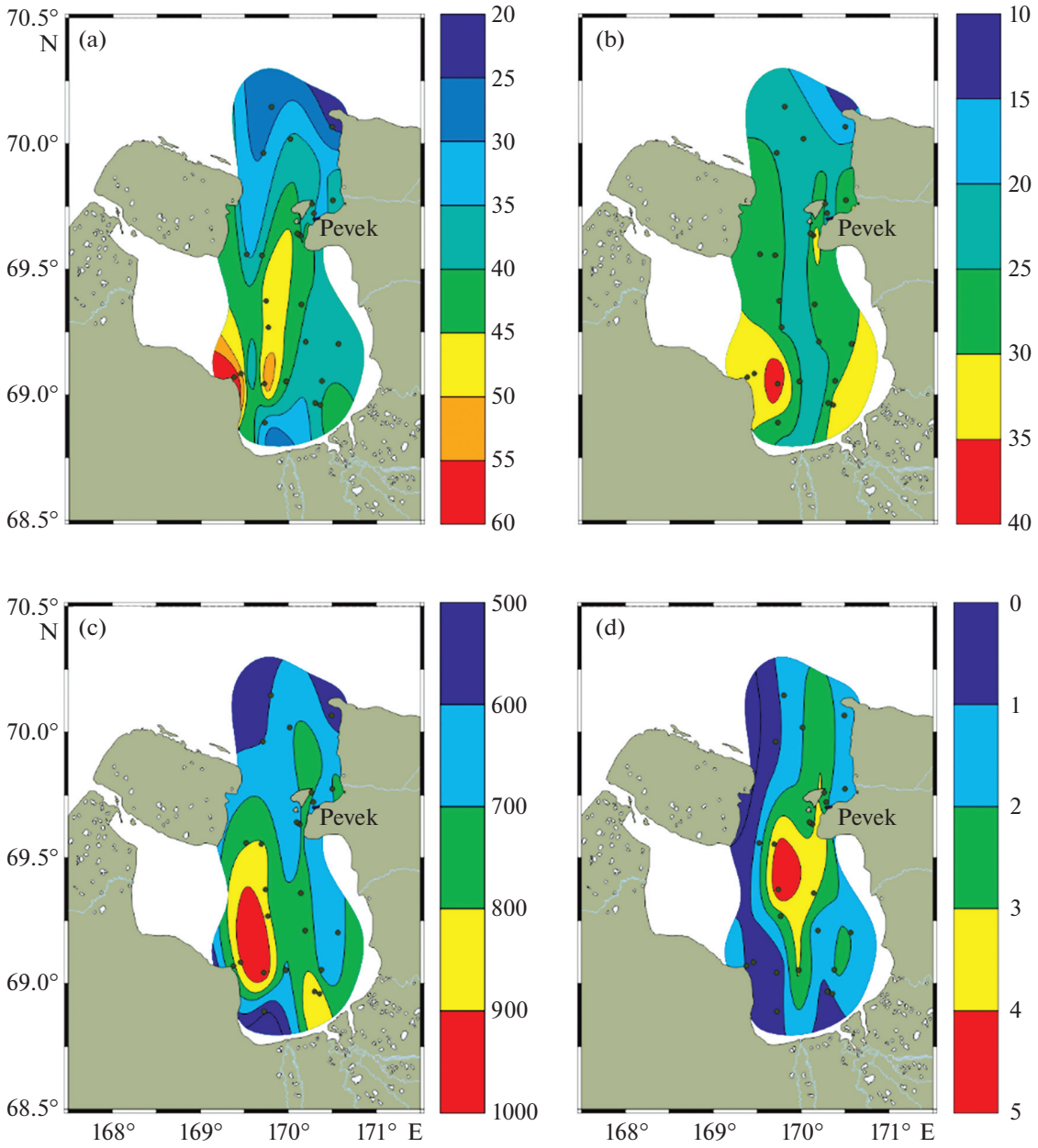

Fig. 3. Surface distributions of active concentrations of ^{232}Th (a), ^{226}Ra (b), ^{40}K (c), and ^{137}Cs (d) radionuclides in studied bottom sediments.

size were common. Such zoning was associated with isolation from the influence of river runoff and thermal abrasion and related to currents that promoted hydrodynamic sorting of the finest-grained fractions. The main area of the central and neck parts of the studied basin included sediments of silty-pelitic size. Their distribution was also related to the distance from the influence of river runoff, abrasion, and thermal abrasion. At the same time, the variability of the particle size composition was facilitated by the dynamics of currents, the seasonality of freeze-up, and the aeolian distribution of particles.

RADIONUCLIDES

The active concentration of natural radionuclides measured in sediments ranged from 23.7 to 77.9 (average, 39.2 ± 10) Bq/kg for ^{232}Th, from 16.5 to 39.3 (average, 26.6 ± 4.4) Bq/kg for ^{226}Ra, and from 535 to 991 (average, 726 ± 109) Bq/kg for ^{40}K. The ^{232}Th/^{226}Ra ratio varied from 1.14 to 2.38 (average, 1.50 ± 0.26); the active concentration of ^{137}Cs differed from 0.5 to 4.7 (average, 2.0 ± 1.1) Bq/kg. Schemes of the distribution of activities of the studied radionuclides are shown in Fig. 3. In general, the average mea-

Table 2. Pearson correlation matrix for the studied parameters of bottom sediments in Chaun Bay ($n = 25$)

Parameters	>63 μm	10–63 μm	2–10 μm	<2 μm	^{232}Th	^{226}Ra	^{40}K	^{232}Th/^{226}Ra	^{137}Cs	C_{org}
>63 μm	–									
10–63 μm	**–0.671**	–								
2–10 μm	**–0.895**	0.272	–							
<2 μm	**–0.892**	0.275	**0.984**	–						
^{232}Th	0.406	–0.411	–0.271	–0.303	–					
^{226}Ra	0.380	–0.050	–0.460	–0.463	**0.594**	–				
^{40}K	0.316	–0.332	–0.208	–0.216	**0.550**	**0.678**	–			
^{232}Th/^{226}Ra	0.074	–0.439	0.176	0.140	**0.695**	–0.149	0.115	–		
^{137}Cs	**–0.644**	0.163	**0.752**	**0.698**	0.038	–0.333	–0.091	0.402	–	
C_{org}	**–0.841**	0.366	**0.884**	**0.840**	–0.044	–0.323	–0.203	0.317	**0.738**	–

Significant ($p < 0.05$) correlations are shown in bold.

sured activity of ^{232}Th and ^{226}Ra in sediments of Chaun Bay agreed with the data obtained for the Eastern Arctic shelf (Charkin et al., 2022), as well as with the global average values (UNSCEAR, 2000). The ^{232}Th/^{226}Ra ratio was also consistent with global values, although the measured average active concentration of ^{40}K in sediments of Chaun Bay was 1.8 times higher compared to the East Siberian Sea (Charkin et al., 2022) and the global level (UNSCEAR, 2000).

In the southwestern part of the bay, in which sediments of sandy and silty-sandy sizes were concentrated, the maximum ^{232}Th activity (stations 67 and 82), ^{226}Ra (stations 67, 69, and 82), and ^{40}K (stations 67 and 69) was observed. Increased ^{232}Th (> 45 Bq/kg) activity was recorded in the central area of the bay (stations 57 and 61). Increased ^{226}Ra (>30 Bq/kg) activity was determined in the southeastern part (station 77), while that of ^{40}K (>800 Bq/kg) was shown in the central and southeastern areas (stations 61, 63, and 77). The northern and southern areas of the bay were characterized by reduced activity of natural radionuclides. The ^{232}Th/^{226}Ra ratio was >1.0 in all studied sediments. The ^{232}Th/^{226}Ra maximum was also recorded at station 82, while increased values were determined in the central area of the bay (stations 57 and 61). For the studied bottom sediments, an increase in the activity of natural radionuclides was noted with increasing concentration of the sand fraction. At the same time, the maximum ^{137}Cs activity was determined in the sediments from the central area of Chaun Bay, which contained clay and silty clay, indicating that ^{137}Cs was concentrated in the clay fraction.

CORRELATION ANALYSIS

The correlation analysis results are shown in Table 2. For the studied marine sediments, a significant ($p < 0.05$) negative relationship was noted between the percentage contribution of sand (>63 μm) and other size fractions (in the >63 μm–10–63 μm, >63 μm–2–10 μm, and >63 μm–<2 μm pairs, $r = –0.67$, –0.89, and –0.89, respectively), as well as with ^{137}Cs and C_{org}. Probably, the former showed the weight antagonism of sand and finer fractions, while the latter indicated that ^{137}Cs and organic matter were concentrated mainly in fine-grained fractions. The latter was confirmed by the positive correlation of ^{137}Cs and C_{org} with 2–10 μm ($r = 0.75$ and 0.88, respectively) and <2 μm ($r = 0.70$ and 0.84, respectively). At the same time, a significant correlation between the 2–10 μm and <2 μm fractions ($r = 0.98$) reflected their related genesis and equal contribution to the sediment mass.

Among natural radionuclides, positive linear correlations of ^{232}Th with ^{226}Ra ($r = 0.59$), ^{40}K ($r = 0.55$), and the ^{232}Th/^{226}Ra ratio ($r = 0.69$), as well as in the ^{226}Ra–^{40}K pair ($r = 0.68$), were noted. This is generally characteristic of the seas of the East Arctic shelf (Charkin et al., 2022). The ^{232}Th–^{232}Th/^{226}Ra correlation indicated the determining contribution of thorium isotopes to the ^{232}Th/^{226}Ra ratio. The positive ^{137}Cs–C_{org} correlation ($r = 0.74$) could be due to the common affinity of organic matter and ^{137}Cs for clay minerals concentrated in the fine-grained fraction of sediments. It should be noted that for natural radionuclides, no significant linear correlation with any of the

Table 3. Values of factor loadings of measured parameters of bottom sediments in Chaun Bay ($n = 25$)

Parameter	F1	F2	F3	F4
>63 μm	**0.949**	0.072	−0.286	−0.041
10–63 μm	−0.482	−0.479	**0.530**	0.467
2–10 μm	**−0.944**	0.205	0.056	−0.214
<2 μm	**−0.931**	0.162	0.055	−0.246
^{232}Th	0.422	**0.840**	0.127	0.297
^{226}Ra	**0.593**	0.261	**0.718**	0.057
^{40}K	0.438	**0.531**	**0.521**	−0.419
^{232}Th/^{226}Ra	−0.086	**0.845**	−0.423	0.260
^{137}Cs	**−0.748**	0.449	−0.006	0.020
C_{org}	**−0.878**	0.327	0.133	0.119

Significant factor loadings are highlighted in bold.

studied particle size fractions was found. This might be due to the diversity of sedimentation environments in Chaun Bay, the pronounced polymictic nature of bottom sediments, and their different origin. Nevertheless, the general trend of a joint increase in the activity of natural radionuclides in the studied bottom sediments was statistically confirmed.

FACTOR ANALYSIS

The factor analysis results are shown in Table 3. For factor F1, which explains 49.5% of the variance, significant positive loadings were noted for >63 μm and ^{226}Ra, while the negative ones were shown for 2–10, <2 μm, ^{137}Cs, and C_{org}. Significant values of factor loadings of 2–10 μm (−0.94) and <2 μm (−0.93) indicated not only their equal mutual contribution but also related (clastic) origin in the sediments, which agreed with the high value of the Pearson correlation coefficient between these fractions ($r = 0.98$). The significant positive F1 loading for >63 μm (0.95) confirmed the antagonism of the weight contribution of sand in sediments compared to fine-grained fractions. Significant negative loadings of ^{137}Cs and C_{org} (−0.75 and −0.88, respectively), along with their negative correlation with sand content ($r = -0.64$ and −0.84, respectively), confirmed that radiocesium and OM were concentrated in clay fractions of sediments (Koarashi et al., 2016; Basuki et al., 2018; Miroshnikov et al., 2020; Budko et al., 2022).

Although ^{226}Ra showed a weak correlation with the particle size distribution of bottom sediments, it had a significant F1 factor loading (0.59). For ^{232}Th and ^{40}K, these values were lower (0.42 and 0.44, respectively); however, their positive values (close to 0.5) allowed a conclusion that natural radionuclides were predominantly concentrated in the sandy fraction of sediments. At the same time, a decreasing linear correlation between the activities of ^{232}Th, ^{226}Ra, and ^{40}K was probably caused by regional features of sedimentation in Chaun Bay. In general, the factor analysis results agreed with the\correlation analysis results and made it possible to conclude that factor F1, which separated most of the analyzed parameters, was lithogenic, reflecting the genesis of sedimentary matter and spatial variability of sedimentation mechanisms (thermal abrasion, coastal abrasion, and river runoff).

Factor F2 explained 23.8% of the variance. Significant positive loadings were shown for ^{232}Th, ^{40}K, and the ^{232}Th/^{226}Ra ratio. The positive correlation in the ^{232}Th–^{232}Th/^{226}Ra pair ($r = 0.69$) confirmed the relatively uniform contribution of ^{232}Th and ^{226}Ra, regardless of the particle size characteristics of bottom sediments. The positive loading of ^{40}K could be explained by the associated accumulation of this radionuclide together with ^{232}Th ($r = 0.55$). In contrast to F1, F2 was a concentration factor associated with varying levels of ^{232}Th and ^{40}K binding to the mineral matrix. Figure 4 shows the surface distributions of the mass content of the >63 μm fraction, the active concentration of ^{232}Th, and the corresponding F1 and F2 values.

Significant positive loadings of the third factor (F3), explaining 13.7% of the variance, were shown for the ^{226}Ra and ^{40}K radionuclides, as well as for the 10–63 μm fraction. As in the case of F2, there was a coaccumulation of ^{226}Ra and ^{40}K ($r = 0.68$). The meaning of factors F3 and F2 was similar. The division of radionuclides into factor groups was caused by the disunity of their concentration on the mineral matrix of different size fractions of sediments. For factor F4, with an explained variance of 6.7%, no significant factor loadings were found.

For the 10–63 μm fraction, quite significant values of F1–F4 factor loadings were observed. The only significant correlation with sand concentration ($r = -0.67$) was less pronounced compared to 2–10 μm and <2 μm. This was due to the characteristics of the genesis and distribution of particles of this dimension. For example, in cryogenic deposits, the mass content and composition of 10–63 μm particles commonly referred to as the "loess" fraction, were informative as an indicator of their aeolian origin (Schirrmeister et al., 2003; Strauss et al., 2012). The polygonal tundra landscape developed in the western and southern parts of Chaun Bay contributes to the influx of sandy and coarse silt particles into sediments as a result of the discharge of coastal permafrost. The distribution of the coarse silt fraction also involves aeolian and ice transport, which is seasonal.

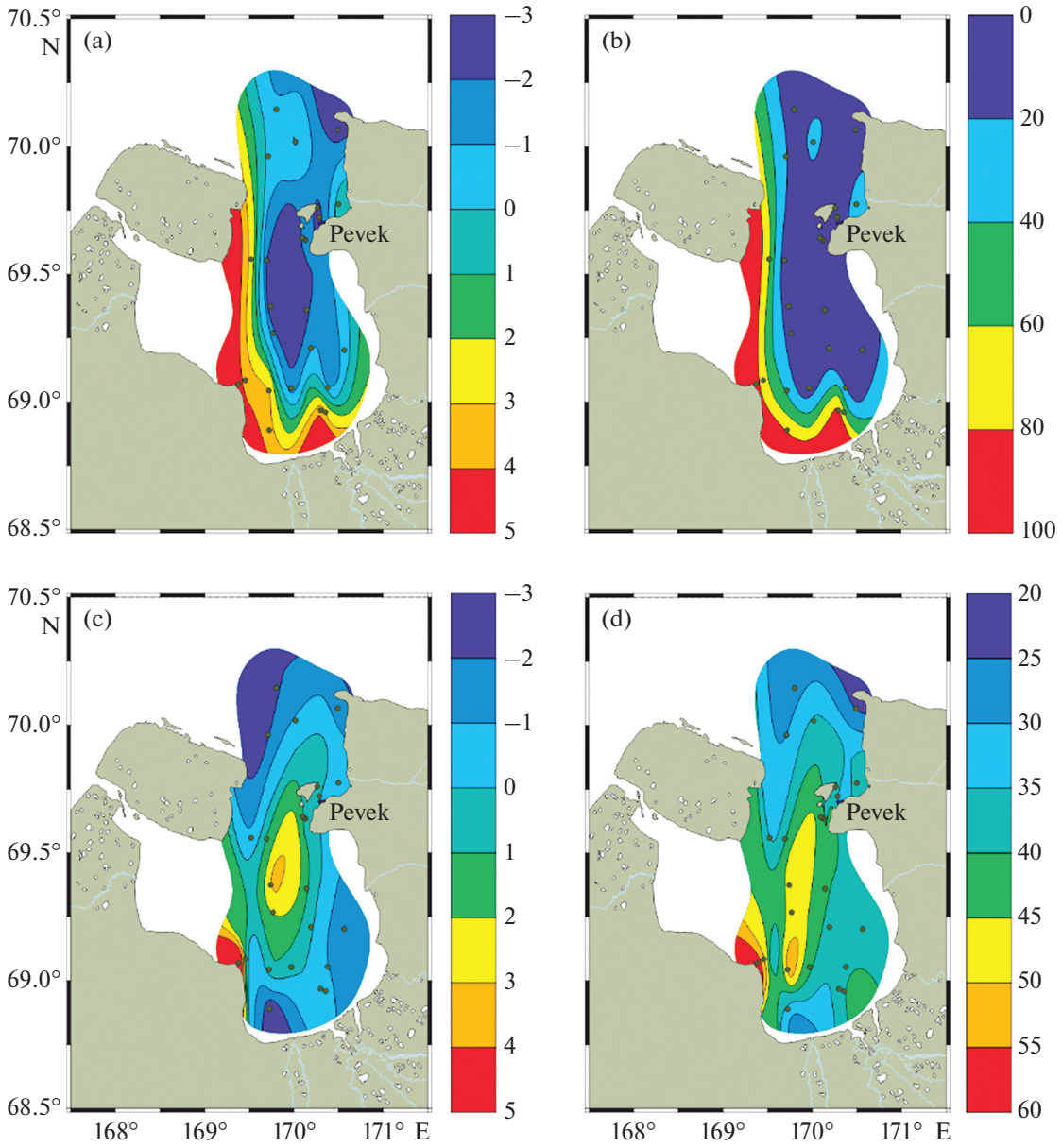

Fig. 4. Surface distributions of F1 values (a), mass content of >63 μm fraction (b), F2 (c), and active concentration of ^{232}Th (d) in studied bottom sediments.

CONCLUSIONS

The data obtained in this study made it possible to characterize the spatial variability of the activity of natural and anthropogenic radionuclides in the surface bottom sediments of Chaun Bay of the East Siberian Sea. This variability is associated with the particle size distribution of bottom sediments and OM concentration. It is governed by the regional physical and geographical features of the studied water area and the sedimentation mode of individual areas of the bay. The results of statistical analysis of the obtained data showed that the dynamics of river runoff, thermal abrasion, and currents, as well as aeolian and ice transport of sedimentary matter, were the main factors determining the differences in the behavior of the studied radionuclides in the surface bottom sediments of Chaun Bay.

The study revealed an increase in the activity of natural radionuclides with increasing activity of ^{40}K radionuclides, which was not previously shown for marine sediments of the Russian Arctic seas. Probably, this was caused by the influx of rock fragments enriched in ^{232}Th, ^{226}Ra, and ^{40}K into the sediments (e.g., feldspars, granitoids, and shales). Differences in the behavior of natural radionuclides in sediments might also be due to exchange between the water col-

umn and the mineral matrix (Webster and Hancock, 1995), leading to an altered $^{232}Th/^{226}Ra$ ratio, as previously shown for submarine groundwater discharge (Charkin et al., 2017, 2020).

The level of radiocesium showed the absence of local sources of anthropogenic pollution in Chaun Bay; however, an increase in ^{137}Cs activity and OM concentration was observed in sediments with a high content of clay fraction. The identified ^{137}Cs–clay–C_{org} correlation triad confirmed an active interaction of radiocesium with organic matter and clay minerals (Johnson-Pyrtle and Scott, 2001; Koarashi et al., 2016; Basuki et al., 2018; Budko et al., 2022). It may be associated, e.g., with coprecipitation of ^{137}Cs radionuclides in complex with humic acids or clay colloids (Shaban and Macášek, 1998).

FUNDING

The study was supported by the Russian Science Foundation, project no. 19-77-10044. The expedition was financed under the state assignment of the Shirshov Institute of Oceanology, Russian Academy of Sciences (topic no. FMWE-2024-0019).

CONFLICT OF INTEREST

The authors of this work declare that they have no conflict of interest.

REFERENCES

Abbasi, A., Cs distribution in the South Caspian region, transfer to biota and dose rate assessment, *Int. J. Environ. Anal. Chem.*, 2019, vol. 100, no. 5, pp. 576–590.

Abbasi, A., Zakaly, H.M.H., and Mirekhtiary, F., Baseline levels of natural radionuclides concentration in sediments yast coastline of North Cyprus, *Mar. Pollut. Bull.*, 2020, vol. 161, 111793.

Abbasi, A., Zakaly, H.M.H., Algethami, M., and Abdel-Hafez, S.H., Radiological risk assessment of natural radionuclides in the marine ecosystem of the northwest Mediterranean Sea, *Int. J. Radiat. Biol.*, 2022, vol. 98, no. 2, pp. 205–211.

Abril, J.M. and Fraga, E., Some physical and chemical features of the variability of Kd distribution coefficients for radionuclides, *J. Environ. Radioact.*, 1996, vol. 30, no. 3, pp. 253–270.

Alshahri, F., Radioactivity of ^{226}Ra, ^{232}Th, ^{40}K and ^{137}Cs in beach sand and sediment near to desalination plant in eastern Saudi Arabia: Assessment of radiological impacts, *J. King Saud Univ. Sci.*, 2017, vol. 29, no. 2, pp. 174–181.

Basuki, T., Miyashita, S., Tsujimoto, M., and Nakashima, S., Deposition density of ^{134}Cs and ^{137}Cs and particle size distribution of soil and sediment profile in Hibara Lake area, Fukushima: An investigation of ^{134}Cs and ^{137}Cs indirect deposition into lake from surrounding area, *J. Radioanal. Nucl. Chem.*, 2018, vol. 316, no. 3, pp. 1039–1046.

Bröder, L., Andersson, A., Tesi, T., et al., Quantifying degradative loss of terrigenous organic carbon in surface sediments across the Laptev and East Siberian seas, *Global Biogeochem. Cycles*, 2019, vol. 33, no. 1, pp. 85–99.

Budko, D.F., Demina, L.L., Travkina, A.V., et al., The features of distribution of chemical elements, including heavy metals and Cs-137, in Surface Sediments of the Barents, Kara, Laptev and East Siberian seas, *Minerals*, 2022, vol. 12.

Charkin, A.N. and Van Der Loeff M R, S., Discovery and characterization of submarine groundwater discharge in the Siberian Arctic seas: a case study in the Buor-Khaya Gulf, Laptev Sea, *Cryosphere*, 2017, vol. 11, no. 5, pp. 2305–2327.

Charkin, A.N., Pipko, I.I., Pavlova, Y.G., et al., Hydrochemistry and isotopic signatures of subpermafrost groundwater discharge along the eastern slope of the Lena River Delta in the Laptev Sea, *J. Hydrol.*, 2020, vol. 590, 125515.

Charkin, A.N., Yaroshchuk, E.I., Dudarev, O.V., et al., The influence of sedimentation regime on natural radionuclide activity concentration in marine sediments of the East Siberian Arctic Shelf, *J. Environ. Radioact.*, 2022, vols. 253–254, 106988.

Domanov, M.M., Verkhovskaya, Z.I., Ambrosimov, A.K., and Domanova, E.G., Comparative characterization of hydrocarbon structures and ^{232}Th and ^{226}Ra concentrations in Caspian Sea sediments, *Pet. Chem.*, 2014, vol. 54, no. 4, pp. 275–282.

Domanov, M.M., Ambrosimov, A.K., and Novichkova, E.A., Specific features of the 226Ra, 238U, and 232Th distribution in the surface layer of marine sediments under the conditions of active biosedimentation in the Arctic Front Zone, *Radiochemistry*, 2019, vol. 61, no. 5, pp. 632–636.

Dudarev, O.V., Charkin, A.N., Shakhova, N.E., et al., *Sovremennyi litomorfogenez na vostochno-arkticheskom shel'fe Rossii* (Recent Lithomorphogenesis on the East Arctic Shelf of Russia), Tomsk: Izd. TPU, 2016.

Ekosistemy, flora i fauna Chaunskoi guby Vostochno-Sibirskogo moray (Ecosystems, Flora, and Fauna of Chauna Bay, East Siberian Sea), Skarlato, A.O., Ed., St. Petersburg: Zool. Inst. Ross. Akad. Nauk, 1994.

Günther, F., Overduin, P.P., Yakshina, I.A., et al., Observing Muostakh disappear: Permafrost thaw subsidence and erosion of a ground-ice-rich island in response to arctic summer warming and sea ice reduction, *Cryosphere*, 2015, vol. 9, no. 1, pp. 151–178.

Johnson-Pyrtle, A. and Scott, M.R., Distribution of Cs in the Lena River estuary–Laptev Sea system, *Mar. Pollut. Bull.*, 2001, vol. 42, no. 10, pp. 912–926.

Koarashi, J., Nishimura, S., Nakanishi, T., et al., Post-deposition early-phase migration and retention behavior of radiocesium in a litter–mineral soil system in a Japanese deciduous forest affected by the Fukushima nuclear accident, *Chemosphere*, 2016, vol. 165, pp. 335–341.

Ligero, R.A., Ramos-Lerate, I., Barrera, M., and Casas-Ruiz, M., Relationships between sea-bed radionuclide activities and some sedimentological variables, *J. Environ. Radioact.*, 2001, vol. 57, no. 1, pp. 7–19.

Lobkovsky, L.I., Nikiforov, S.L., Shakhova, N.E., Semiletov, I.P., Libina, N.V., Ananiev, R.A., and Dmitrevskii, N.N., Mechanisms responsible for degradation of submarine permafrost on the eastern arctic shelf of Russia, *Dokl. Earth Sci.*, 2013, vol. 449, no. 1, pp. 280–283.

Mehnati, P., Jomehzadeh, A., and Doostmohammadi, V., Measurement of 226Ra, ^{232}Th, ^{40}K and ^{137}Cs concentrations in sediment samples and determination of annual effective dose due to these radionuclides in vicinity of hot springs in Kerman Province, *Int. J. Radiat. Res.*, 2022, vol. 20, no. 1, pp. 223–228.

Miroshnikov, A.Yu., Radiocaesium distribution in the bottom sediments of the Kara Sea, *Geoekol., Inzh. Geol., Gidrogeol., Geokriol.*, 2012, no. 6, pp. 540–550.

Miroshnikov, A.Yu., Laverov, N.P., Chernov, R.A., et al., Radioecological investigations on the Northern Novaya Zemlya Archipelago, *Oceanology*, 2017, vol. 57, no. 1, pp. 204–214.

Miroshnikov, A.Yu., Flint, M.V., Asadulin, En.E., and Komarov, Vl.B., Radiation-geochemical dtability of bottom sediments in the Ob and Yenisei estuaries and adjacent shoal area of the Kara Sea, *Oceanology*, 2020, vol. 60, no. 6, pp. 817–830.

Miroshnikov, A.Yu., Flint, M.V., Asadulin, E.E., et al., Ecological state and mineral-geochemical characteristics of the bottom sediments of the East Siberian Sea, *Oceanology*, 2020, vol. 60, pp. 518–531.

Nguyen, T., Tran, Q., Nguyen, V., et al., Activity concentrations of Sr-90 and Cs-137 in seawater and sediment in the Gulf of Tonkin, Vietnam, *J. Chem.*, 2020, 8752606.

Overduin, P.P., Strzelecki, M.C., Grigoriev, M.N., et al., Coastal changes in the Arctic, in *Sedimentary Coastal Zones from High to Low Latitudes: Similarities and Differences. Spec. Publ.–Geological Society London*, Martini, I.P. and Wanless, H.R., Eds., 2014, vol. 388, no. 1, pp. 103–129.

Sarkisov, A.A., The question of clean-Up of radioactive contamination in the Arctic Region, *Herald Russ. Acad. Sci.*, 2019, vol. 89, no. 1, pp. 7–22.

Schirrmeister, L., Grosse, G., Schwamborn, G., et al., Late Quaternary history of the accumulation plain north of the Chekanovsky Ridge (Lena delta, Russia): A multidisciplinary approach, *Polar Geogr.*, 2003, vol. 27, no. 4, pp. 277–319.

Shaban, I.S. and Macášek, F., Influence of humic substances on sorption of cesium and strontium on montmorillonite, *J. Radioanal. Nucl. Chem.*, 1998, vol. 229, nos. 1–2, pp. 73–78.

Shakhova, N., Semiletov, I., Gustafsson, O., et al., Current rates and mechanisms of subsea permafrost degradation in the East Siberian Arctic Shelf, *Nat. Commun.*, 2017, vol. 8, no. 1, 15872.

Strauss, J., Schirrmeister, L., Wetterich, S., et al., Grain-size properties and organic-carbon stock of Yedoma Ice Complex permafrost from the Kolyma lowland, northeastern Siberia, *Global Biogeochem. Cycles*, 2012, vol. 26, no. 3, GB3003.

Stremyakov, A.Ya., On the problem of the origin of oriented lakes, in *Mnogoletnemerzlye gornye porody razlichnykh raionov SSSR* (Permafrost Rocks of Various Regions of Soviet Union), Moscow: Izd. Akad. Nauk SSSR, 1963, pp. 75–107.

Ulyantsev, A.S., Bratskaya, S.Yu., and Privar, Yu.O., Grain size properties of the bottom sediments from Buor-Khaya Bay, *Oceanology*, 2020, vol. 60, no. 3, pp. 452–465.

Ulyantsev A.S., Charkin, A.N., Syomin, V.L., et al., Geological studies of the upper sedimentary strata of Chaun Bay during cruise 60 of the R/V *Akademik Oparin, Oceanology*, 2021, vol. 61, pp. 584–585.

UNSCEAR. Sources and Effects of Ionizing Radiation, Report to the General Assembly with Scientific Annexes. Vol. 1, NY, USA: United Nation, 2000.

Vonk, J.E., Sánchez-García, L., Van Dongen, B.E., et al., Activation of old carbon by erosion of coastal and subsea permafrost in Arctic Siberia, *Nature*, 2012, vol. 489, no. 7414, pp. 137–140.

Wester, I.T., Hancock, G.J., and Murray, A.S., Modelling the effect of salinity on radium desorption from sediments, *Geochim. Cosmochim. Acta*, 1995, vol. 59, no. 12, pp. 2469–2476.

Yushin, N., Jakhu, R., Chaligava, O., et al., Natural and anthropogenic radionuclides concentration with heavy metals analysis of the sediments collected around Novaya Zemlya, *Mar. Pollut. Bull.*, 2023, vol. 194, 115346.

Translated by A. Panyushkina